A Reverse-Coupled Bipolar Coil Structure for an Integrated LCC-Compensated Inductive Power Transfer System

Fei Lu[1], *Member, IEEE*, Hua Zhang[1], *Member, IEEE*, Chong Zhu[1], Ying Mei[2], Jie Zhang[2], Chris Mi[1,*], *Fellow, IEEE*
[1] San Diego State University, San Diego, CA, 92182, USA
[2] LG Electronics, Shanghai, 201206, China
[*]Email: mi3032@gmail.com

***Abstract*—This paper proposes a reverse-coupled bipolar coil structure to realize an integrated LCC-compensated inductive power transfer (IPT) system. Two unipolar coils are connected reversely, resulting in a bipolar structure, which is used as the compensation inductor in an LCC-compensated IPT system. This bipolar coil is integrated into the main coil to save space, and its dimensions are designed to eliminate its magnetic coupling with the same-side main coil and simplify the circuit analysis. The working principle of the integrated IPT system is presented, which shows that the proposed bipolar coil can help improve the system performance with position and angular misalignment in the horizontal plane. A prototype is designed and implemented to validate the proposed bipolar coil structure. The primary coil dimension is 450mm×450mm, and the secondary coil size is 300mm×300mm. Experiments show that it can achieve 2.15kW power transfer with 89.9% dc-dc efficiency across an airgap of 200mm. When there is 150mm misalignment, the system power and efficiency are not significantly affected, and it can still maintain 80.5% of the well-aligned power with 89.0% efficiency.**

Keywords—inductive power transfer (IPT), unipolar coil structure, bipolar coil structure, integrated magnetic coupler, double-sided LCC compensation, reverse-coupled.

I. INTRODUCTION

Inductive power transfer (IPT) technology utilizes high-frequency magnetic fields to transfer power without any galvanic contact, which has been widely used in the mobile device and electric vehicle charging applications [1]-[2]. The design objective of an IPT system can be summarized as five parts: high power, high efficiency, compact size, acceptable safety, and good misalignment. To realize these targets, the recent study of the IPT technology mainly includes three directions: the system structure design and optimization [3]-[4], the compensation circuit topology design [5]-[6], and the magnetic coupler structure design [7]-[8].

First, the system structure design requires to optimizing the number of power electronics stages [9]. More power converters can provide the flexibility to control the system performance, but it increases the system size and induces more cost. For example, a DC/DC converter at the vehicle side can contribute to regulate the charging current to the batteries. However, this converter needs to occupy the valuable space at the vehicle side, which is usually eliminated in the practical application.

Second, the compensation circuit design of an IPT system has been well investigated. The basic compensation topology consists of a single capacitor at each side, which can be connected in series or parallel with the power transfer coils, resulting in SS (series-series), SP (series-parallel), PS(parallel-series), and PP (parallel-parallel) structures [10]-[11]. The SS compensation has been widely applied in practice because of its simplicity. However, its limitation is that the output power is inversely proportional to the coupling coefficient. The LCC compensation circuit is proposed that can provide proportional output power with respect to the coupling. Also, it has a constant-current output property, which is suitable for battery charging application [12]. Therefore, this topology is getting more attention in the practical applications.

Third, the magnetic coupler design focuses on the coil structure, which usually consists of two different types: bipolar and unipolar [13]. The bipolar coil contains two unipolar ones with opposite current directions. The recent bipolar coils are mainly in a DD structure, in which two unipolar coils are placed adjacent to each other [14]-[15]. Based on the DD coils structure, one important research direction is to combine the magnetic coupler design with the compensation circuit design. Since there are more passive components in an LCC circuit, it is meaningful to integrate these compensation inductors into the mains to save space, resulting in an integrated magnetic coupler [16]-[17]. In the previous design, the compensation inductors are designed in a DD structure and the main coils are in unipolar shape to simplify the couplings in the magnetic coupler [18]-[19]. Although it has been proven that the position misalignment performance can be improved [20]-[21], the angular misalignment performance still needs to be improved, which means the system power will be significantly reduced if the coils are rotated in the horizontal plane.

This paper proposes a novel reverse-coupled bipolar structure that is used to realize an integrated magnetic coupler structure, and the LCC compensation is also used to realize an IPT system. It contains two reversely connected unipolar coils: one is larger with less turns and the other is smaller with more turns. The smaller unipolar coil is concentrically placed inside of the larger unipolar coil. Since they are essentially two unipolar coils, the new structure is immunized to the angular misalignment, and the system misalignment performance of the IPT system is therefore improved.

II. Integrated LCC-Compensated IPT System

A. Circuit Structure

The circuit topology of an integrated LCC-compensated IPT system is shown in Fig. 1. A full-bridge inverter using MOSFETs is used at the primary side to provide AC excitation, and a full-bridge diode rectifier is used at the secondary side to provide dc current to the load. The inductors L_1 and L_2 represent the main coils, and the other passive components form the compensation circuits.

In Fig. 1, the primary compensation consists of inductors L_{f1a}, L_{f1b} and capacitors C_1, C_{f1}. To reduce the system size, inductors L_{f1a}, L_{f1b} are integrated into the primary main coil L_1, resulting in a primary coupler. Since L_{f1a} and L_{f1b} are arranged at the front-end, they can also provide the benefit to limit the common-mode current injected into the circuit. Similarly, at the secondary side, compensation circuit contains inductors L_{f2a}, L_{f2b} and capacitors C_2, C_{f2}. The inductors L_{f2a}, L_{f2b} are integrated into the secondary main coil L_2 as well, resulting in a secondary coupler.

Since the compensation inductors are integrated with the main coils, there are multiple magnetic couplings in this new integrated coupler. Every two inductors can result in one magnetic coupling, and the six inductors in Fig. 1 can result in fifteen couplings in total, which induce the complexity and difficulty to analyze the working principle of the circuit. Considering the conventional LCC compensation in reference [12] and integrated coupler model in reference [21], the series connected and coupled inductors L_{f1a} and L_{f1b} can be treated as an equivalent front-end inductor L_{f1}. The two separated inductors L_{f2a} and L_{f2b} are connected in series, and they can be treated as an equivalent back-end inductor L_{f2}. The coupling coefficient between L_{f1a} and L_{f1b} is defined as $k_{f1a\text{-}f1b}$, and the coupling coefficient between L_{f2a} and L_{f2b} is defined as $k_{f2a\text{-}f2b}$,

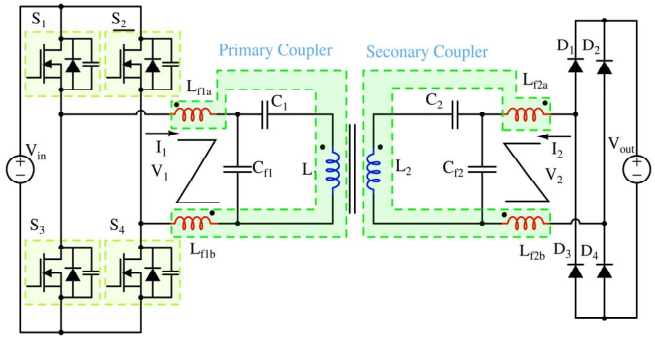

Fig. 1. Circuit topology of an integrated LCC-compensated IPT system

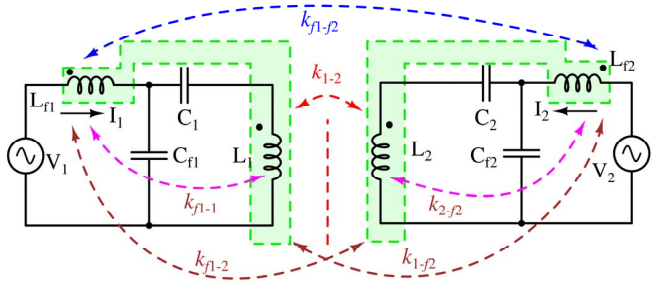

Fig. 2. Equivalent circuit of magnetic couplings in an integrated system

resulting in the primary and secondary equivalent inductances L_{f1} and L_{f2} as calculated in (1).

$$\begin{cases} L_{f1} = L_{f1a} + L_{f1b} + 2k_{f1a-f1b}\sqrt{L_{f1a}L_{f1b}} \\ L_{f2} = L_{f2a} + L_{f2b} + 2k_{f2a-f2b}\sqrt{L_{f2a}L_{f2b}} \end{cases} \tag{1}$$

Therefore, only four inductors need to be considered and there are totally six magnetic couplings. Using fundamental harmonics approximation (FHA) method, the circuit in Fig. 1 can be simplified as an equivalent circuit as shown in Fig. 2.

In Fig. 2, the six coupling coefficients between inductors are defined as $k_{f1\text{-}1}$, $k_{f1\text{-}2}$, $k_{f1\text{-}f2}$, $k_{1\text{-}2}$, $k_{1\text{-}f2}$, and $k_{2\text{-}f2}$. The six mutual inductances are then defined as $M_{f1\text{-}1}$, $M_{f1\text{-}2}$, $M_{f1\text{-}f2}$, $M_{1\text{-}2}$, $M_{1\text{-}f2}$, and $M_{2\text{-}f2}$, resulting in the relationship as in (2).

$$\begin{aligned} &M_{1-2} = k_{1-2}\cdot\sqrt{L_1L_2}, M_{f1-f2} = k_{f1-f2}\cdot\sqrt{L_{f1}L_{f2}} \\ &M_{f1-1} = k_{1-f1}\cdot\sqrt{L_1L_{f1}}, M_{2-f2} = k_{2-f2}\cdot\sqrt{L_2L_{f2}} \\ &M_{1-f2} = k_{1-f2}\cdot\sqrt{L_1L_{f2}}, M_{f1-2} = k_{f1-2}\cdot\sqrt{L_{f1}L_2} \end{aligned} \tag{2}$$

The coupling coefficient $k_{1\text{-}2}$ represents the coupling between coils and dominates the power transfer, which is defined as main coupling; $k_{f1\text{-}f2}$ is defined as compensation coupling; $k_{f1\text{-}2}$ and $k_{1\text{-}f2}$ are defined as cross-couplings; $k_{f1\text{-}1}$ and $k_{2\text{-}f2}$ are defined as same-side couplings. It needs to be pointed out that the same-side couplings $k_{f1\text{-}1}$ and $k_{2\text{-}f2}$ only relates to the reactive power circling in the same side, and they do not contribute to the power transfer process. Therefore, they should be minimized to reduce the reactive power and maintain a high efficiency in the system.

B. Reverse-Coupled Bipolar Coil Structure

The aforementioned same-side couplings $k_{f1\text{-}1}$ and $k_{2\text{-}f2}$ can be minimized by coil structure design. For example, a reverse-coupled bipolar coil structure is shown in Fig. 3, including the inductors L_{f1a}, L_{f1b}, and L_1 at the primary side.

In Fig. 3, the compensation inductors L_{f1a} are L_{f1b} are both in unipolar structure and labeled in red color. The main coil L_1 is also unipolar and labeled in blue color. At the secondary side, similar coil structure is adopted. The size of the secondary coils can be different from that of the primary coils, but they are all unipolar shape. Therefore, when there is angular misalignment, the couplings between the primary and secondary coils do not change too much. However, in a conventional bipolar structure realized by a DD structure [21], the coupling coefficient is sensitive to angular mismatch. The coupling can decrease to 0 with 90° rotation. Therefore, the proposed coupler structure can significantly improve the misalignment performance.

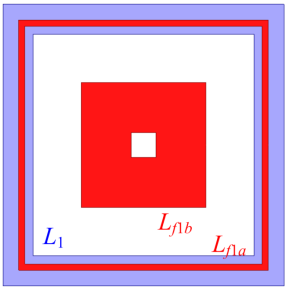

Fig. 3. Structure of an integrated reverse-coupled bipolar coil at primary side

As mentioned above, inductors L_{f1a} and L_{f1b} are connected in series to form an inductor L_{f1} at the primary side. Since the coils are integrated, L_1 has couplings with both L_{f1a} and L_{f1b}, and the mutual inductance $M_{1\text{-}f1}$ between L_1 and L_{f1} can be expressed as in (3).

$$M_{1-f1} = M_{1-f1a} + M_{1-f1b} = k_{1-f1a}\sqrt{L_1 \cdot L_{f1a}} + k_{1-f1b}\sqrt{L_1 \cdot L_{f1b}} \tag{3}$$

To reduce the same-side coupling, the coupler structure can be designed to achieve $M_{1\text{-}f1}$=0, resulting in (4) as below.

$$k_{1-f1a}\sqrt{L_{f1a}} + k_{1-f1b}\sqrt{L_{f1b}} = 0 \tag{4}$$

To clarify, it means as long as the equation (4) is satisfied, the coupling between L_1 and L_{f1} is eliminated. It needs to be pointed out that the conventional DD coil in reference [21] also satisfies equation (4), because there is parameter relationship as L_{f1a}=L_{f1b} and $k_{1\text{-}f1a}$=-$k_{1\text{-}f1b}$.

In this proposed structure of Fig. 3, since L_{f1a} is placed close to L_1, and L_{f1b} is relatively far from L_1, there exist the relationship of couplings: $|k_{1\text{-}f1a}|>|k_{1\text{-}f1b}|$. To satisfy equation (4), it requires $k_{1\text{-}f1a}$ having an opposite sign with $k_{1\text{-}f1b}$, and $L_{f1a}<L_{f1b}$. In a practical application, the outer inductor L_{f1a} has less turns to achieve a small inductance, and the inner inductor L_{f1b} has more turns to achieve a larger inductance. It is concluded that L_{f1a} and L_{f1b} need to be reversely connected, resulting in a reverse-coupled bipolar coil structure.

C. Circuit Working Principle

With the proposed reverse-coupled bipolar structure, the same-side magnetic couplings can be mitigated, resulting in a simplified circuit topology as in Fig. 4.

In Fig. 4, the same-side coupling coefficients $k_{f1\text{-}1}$ and $k_{2\text{-}f2}$ are reduced to zero, and the other coupling coefficient $k_{1\text{-}2}$, $k_{f1\text{-}f2}$, $k_{f1\text{-}2}$, and $k_{1\text{-}f2}$ need to be considered. According to the *Kirchhoff circuit laws* (*KCL*), the circuit relationships can be described as shown in equation (5).

$$\begin{cases} \left(j\omega L_{f1} + \dfrac{1}{j\omega C_{f1}}\right) I_1 - \dfrac{1}{j\omega C_{f1}} I_{L1} + j\omega M_{f1-f2} I_2 + j\omega M_{f1-2} I_{L2} = V_1 \\ -\dfrac{1}{j\omega C_{f1}} I_1 + \left(\dfrac{1}{j\omega C_1} + \dfrac{1}{j\omega C_{f1}} + j\omega L_1\right) I_{L1} + j\omega M_{1-f2} I_2 + j\omega M_{1-2} I_{L2} = 0 \\ j\omega M_{f1-f2} I_1 + j\omega M_{1-f2} I_{L1} + \left(j\omega L_{f2} + \dfrac{1}{j\omega C_{f2}}\right) I_2 - \dfrac{1}{j\omega C_{f2}} I_{L2} = V_2 \\ j\omega M_{f1-2} I_1 + j\omega M_{1-2} I_{L1} + \dfrac{1}{j\omega C_{f2}} I_2 + \left(\dfrac{1}{j\omega C_2} + \dfrac{1}{j\omega C_{f2}} + j\omega L_2\right) I_{L2} = 0 \end{cases} \tag{5}$$

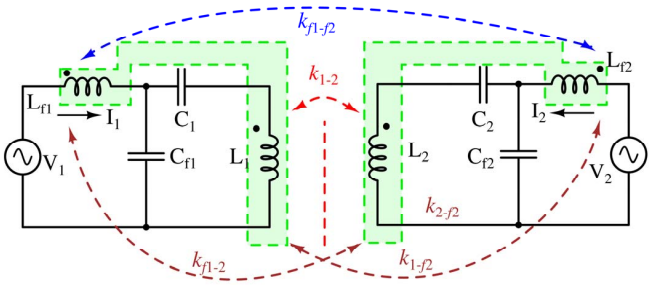

Fig. 4. Simplified circuit topology of an integrated system

According to the reference [21], in a double-sided LCC-compensated IPT system, the circuit parameters can be designed to achieve the resonance relationship described by the following equation.

$$\begin{cases} j\omega L_{f1} + \dfrac{1}{j\omega C_{f1}} = j\omega L_{f2} + \dfrac{1}{j\omega C_{f2}} = 0 \\ \dfrac{1}{j\omega C_1} + \dfrac{1}{j\omega C_{f1}} + j\omega L_1 = \dfrac{1}{j\omega C_2} + \dfrac{1}{j\omega C_{f2}} + j\omega L_2 = 0 \end{cases} \tag{6}$$

By substituting (6) into (5), the circuit description can be simplified as below.

$$\begin{cases} -\dfrac{1}{j\omega C_{f1}} I_{L1} + j\omega M_{f1-f2} I_2 + j\omega M_{f1-2} I_{L2} = V_1 \\ -\dfrac{1}{j\omega C_{f1}} I_1 + j\omega M_{1-f2} I_2 + j\omega M_{1-2} I_{L2} = 0 \\ j\omega M_{f1-f2} I_1 + j\omega M_{1-f2} I_{L1} - \dfrac{1}{j\omega C_{f2}} I_{L2} = V_2 \\ j\omega M_{f1-2} I_1 + j\omega M_{1-2} I_{L1} + \dfrac{1}{j\omega C_{f2}} I_2 = 0 \end{cases} \tag{7}$$

Further simplification of equation (7) can be processed using the following procedures. The input and output voltages V_1 and V_2 are treated as known variables, and the currents I_1, I_2, I_{L1}, and I_{L2} are treated as unknown variables. Considering that there are four unknown variables (7) and (7) can provide four independent equations, it is already sufficient to obtain the system currents. However, it needs to be emphasized that the amplitude of the output voltage V_2 is known and its phase angle with respect to the input voltage V_1 needs to be decided. Since a full-bridge rectifier can be treated as a resistive load at the output side, the output voltage V_2 is in phase with the output current I_1, which provides the fifth equation. In this system, the input and output currents I_1 and I_2 attract more interests. The intermedium currents I_{L1} and I_{L2} do not directly relate to the system power, and they can be eliminated in the calculation process. Then, further calculation of equation (7) can provides the output power of the integrated IPT system as expressed below.

$$P_{out} = \frac{k_{1-2}\sqrt{L_1 L_2}}{\omega L_{f1} L_{f2}} \cdot \frac{1}{1 - K_1 - 3K_2 + 2K_3\gamma} \cdot |V_1| \cdot |V_2| \tag{8}$$

where, the new variables K_1, K_2, K_3, and γ relates to the circuit parameters and magnetic coupling coefficients, and they can be expressed as below.

$$\begin{cases} K_1 = k_{1-2} k_{f1-f2} \beta \\ K_2 = k_{f1-2} k_{1-f2} \beta \\ K_3 = k_{f1-2} k_{f1-2} \beta \\ \beta = \dfrac{\sqrt{L_1 L_2}}{\sqrt{L_{f1} L_{f2}}}, \gamma = \dfrac{L_{f1}}{L_{f2}} \cdot \dfrac{\sqrt{L_{f1} L_2}}{\sqrt{L_{f2} L_1}} \end{cases} \tag{9}$$

Compared to the output power of a conventional double-sided LCC-compensated IPT system without integration [12], it shows that the parameters K_1, K_2, and K_3 have the capability to improve the misalignment performance. For example, when there is misalignment, the $k_{1\text{-}2}$ will decrease, leading to a decrease of system power. However, the parameters can be designed to achieve an increasing K_1, K_2, and a decreasing K_3, and the system power decrease is therefore alleviated.

III. A Design Example of Reverse-Coupled Bipolar Magnetic Coupler

The 3-D view of a reverse-coupled bipolar coupler is shown in Fig. 5. The main coils L_1 and L_2, the compensation inductors L_{f1a}, L_{f1b}, L_{f2a}, and L_{f2b} are all labeled to show their relative position arrangement. To simplify the design process, the magnetic coupler is set in square shape in this design. It needs to be pointed out that the shape of coupler can vary depending on the practical requirements.

In Fig. 5, the main coils are set to be in blue color, and the compensation coils are set to be in red color. At the primary side, the compensation coil L_{f1a} is placed close to the main coil L_1 to maintain a relatively large coupling coefficient. They can be arranged in different horizontal planes, resulting in a double layer coil structure. While, they can also be arranged in the same horizontal plane to reduce the coil thickness. Similar design can be performed for the secondary coils.

In this design, the airgap distance is set as 200mm, the length of primary coil is defined as l_1=450mm, and the length of secondary coil is defined as l_2=300mm. Then, the widths of windings in the coils need to be determined. Here, at the primary side, the winding width of L_1 is defined as w_1, and the width ratio is defined as $r_{L1}=w_1/l_1$. At the secondary side, the winding ratio of L_2 is defined as w_2, and the corresponding width ratio is defined as $r_{L2}=w_2/l_2$. According to Maxwell simulation [21], a large value of width ratio r_{L1} can affect the misalignment performance. Therefore, r_{L1} is selected as 0.12 for a good misalignment ability. When r_{L2} varies, the Maxwell-simulated coupling coefficient $k_{1\text{-}2}$ is shown in Fig. 6.

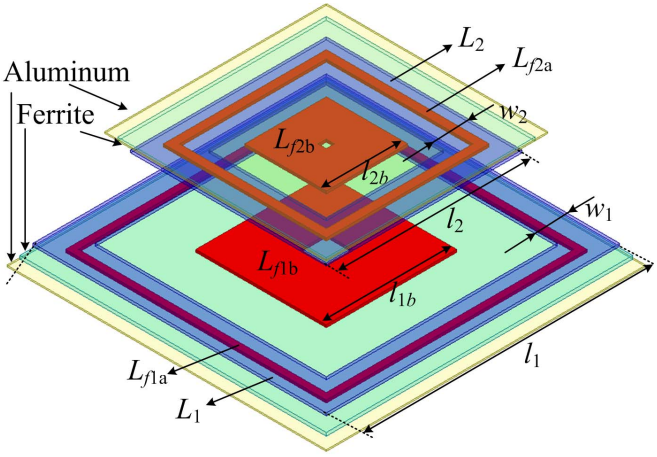

Fig. 5. 3-D view of a reverse-coupled bipolar coupler structure

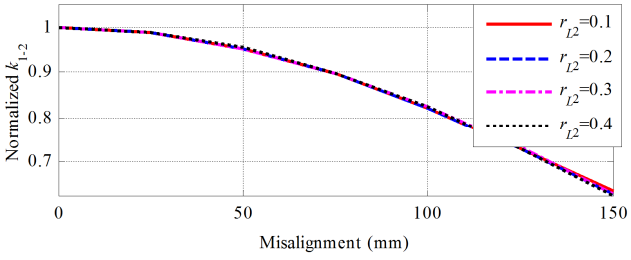

Fig. 6. Maxwell-simulated normalized $k_{1\text{-}2}$ at different width ratio r_{L2}

Fig. 6 shows the normalized coupling coefficient with the maximum value as the nominal reference. It indicates that when there is 150mm misalignment, the main coupling $k_{1\text{-}2}$ will reduces to 62% of the well-aligned value. Since the output power of a single-coupled LCC-compensated IPT system is proportional to the coupling coefficient [12], the system power will also drops to 62% of the well-aligned power.

After the main coils L_1 and L_2 are determined, the other compensation inductors L_{f1a}, L_{f1b}, L_{f2a}, and L_{f2b} need to be designed. It should be pointed out that the inner inductors L_{f1b} and L_{f2b} dominate the equivalent compensation inductance L_{f1} and L_{f2}. To limit their coupling with the same-side main coils, their lengths should be designed to be much smaller than the corresponding main coils. For example, the dimensions can be l_{1b}=225mm and l_{2b}=100mm in Fig. 5. After that the length of the other two compensation inductors L_{f1a} and L_{f2a} should be designed to satisfy equation (4).

IV. Prototype Design and Experiments

A. Prototype Design

A prototype of the proposed reverse-coupled bipolar coupler structure is implemented, and the coils are shown in Fig. 7. The size of the main coils and inductors are also labeled in the figure. To reduce the thickness of the coil, the main coil and inductor are wound in the same horizontal plane. To summarize, at the primary side, there are l_1=450mm, l_{1a}=350mm, and l_{1b}=225mm. While, at the secondary side, there are l_2=300mm, l_{2a}=200mm, and l_{2b}=100mm.

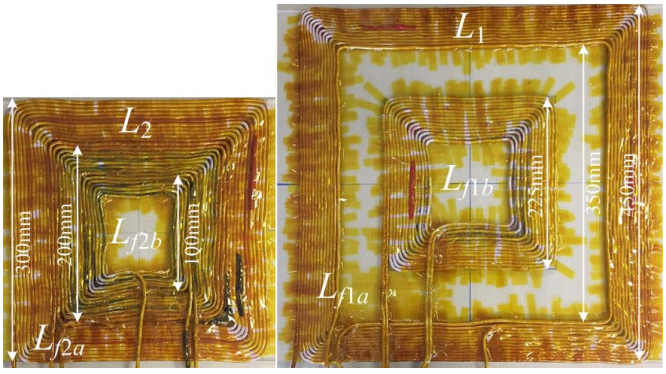

Fig. 7. Prototype of a reverse-coupled bipolar coupler

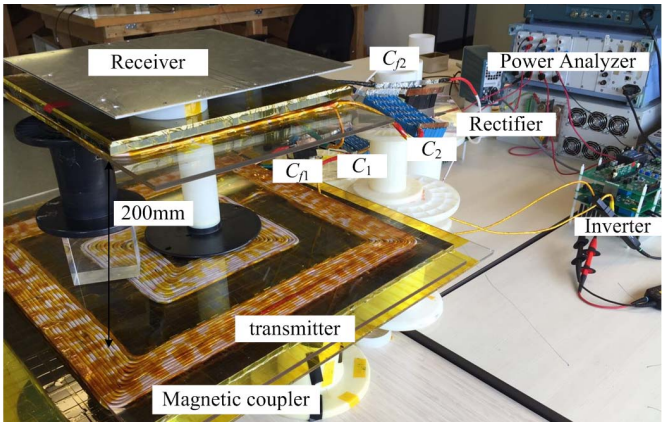

Fig. 8. An integrated IPT system with the reverse-coupled bipolar coupler

The designed two coils are used to build a magnetic coupler with the ferrite and aluminum sheets, and the inductances and coupling coefficient can be then measured. The measurement shows that the two primary compensation inductances as L_{f1a}=20.0μH, L_{f1b}=2.06μH, $k_{1\text{-}f1a}$=0.20, and $k_{1\text{-}f1b}$=0.64. When L_{f1a} and L_{f1b} are reversely connected, the measurement further shows that the equivalent inductances L_{f1} satisfies equation (4), which results in L_{f1}=20.0μH. Similarly, at the secondary side, the measurement shows L_{f2a}=11.14μH, L_{f2b}=3.63μH, $k_{2\text{-}f2a}$=0.38, and $k_{2\text{-}f2b}$=0.68. Also, if L_{f2a} and L_{f2b} are reversely connected, the measurement shows that the equivalent inductance L_{f2} satisfies equation (4). It means L_{f2} and L_2 have no coupling and there is L_{f2}=11.44μH.

Using the designed magnetic coupler, an integrated IPT system is constructed as shown in Fig. 8. The self-inductances of the main coils are measured as L_1=214.7μH, L_2=147.1μH. According to the resonance relationships in equation (6), the compensation capacitances can be calculated as C_1=18.0nF, C_2=25.8nF, C_{f1}=177nF, C_{f2}=307nF. Since the airgap distance is 200mm and the compensation coils are relatively small, measurements show that $k_{1\text{-}2}$=11.0% and $k_{f1\text{-}2}$=5.4%, and the other coupling coefficients are too small to be neglected in the well-aligned case. Therefore, according to equation (9), there are K_1=K_2=0, K_3=0.08, β=11.7, and γ=1.91. When there is 150mm misalignment, the measurement shows that K_3 decreases to a value very close to zero. According to the power equation (7), a decreasing K_3 can contribute to improve the system misalignment performance.

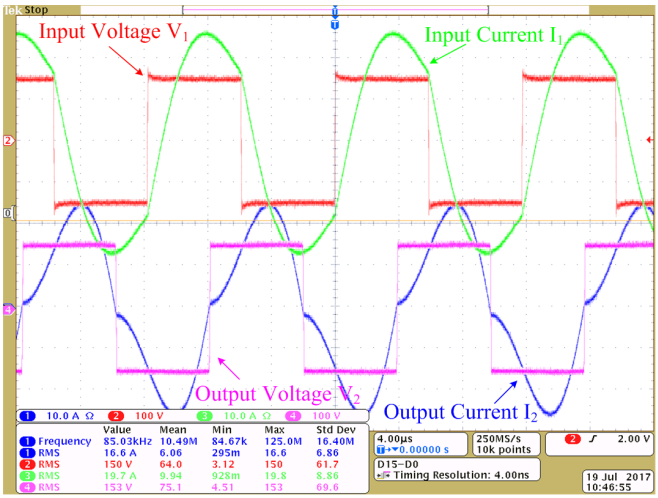

Fig. 9. Experimental waveforms at well-aligned case

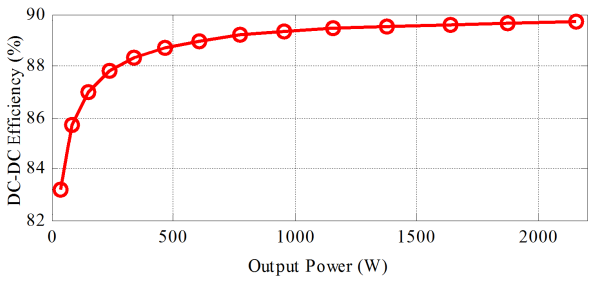

Fig. 10. Output power and efficiency at well-algined case

B. *Experimental Results*

The well-aligned experiments are conducted first. When the input and output voltages increase to 220V, the experimental waveforms are shown in Fig. 9. It indicates that near unity power factor is achieve at both the input and output side. At the primary side, it shows that the input current I_1 is slightly lagging the input voltage V_1, which is used to achieve soft-switching of the MOSFETs. In this well-aligned case, when the input voltage increases all the way from zero to 220V, the output power and dc-dc efficiency are both measured as shown in Fig. 10. It shows that as long as the output power reaches 300W, the system can maintain a dc-dc efficiency higher than 88%. When the voltage reaches 220V, the system can achieve 2.15kW power transfer with a dc-dc efficiency of 89.9%.

The system is also tested in misaligned cases, and the experimental waveforms with 220V input and output voltages

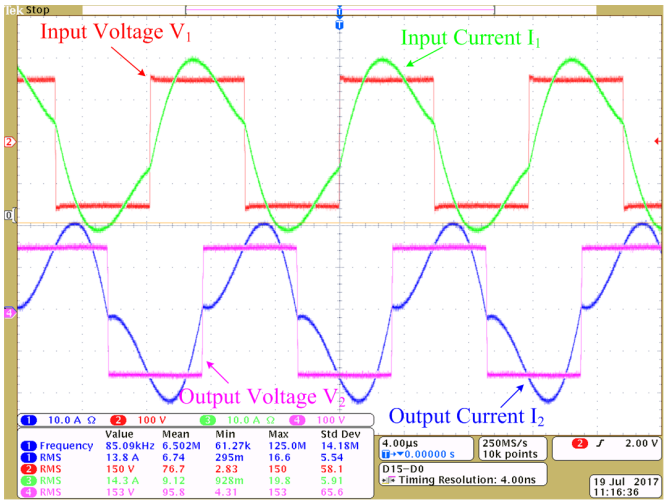

Fig. 11. Experimental waveforms at 150mm misalignment case

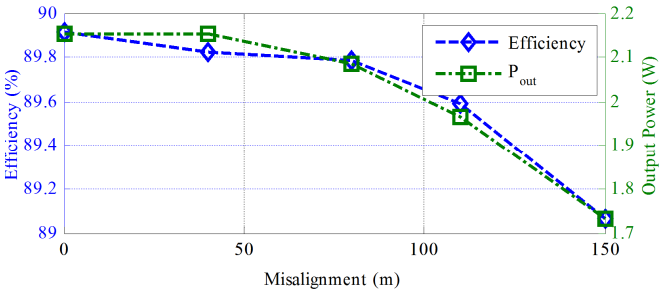

Fig. 12. Output power and efficiency at misaligned case

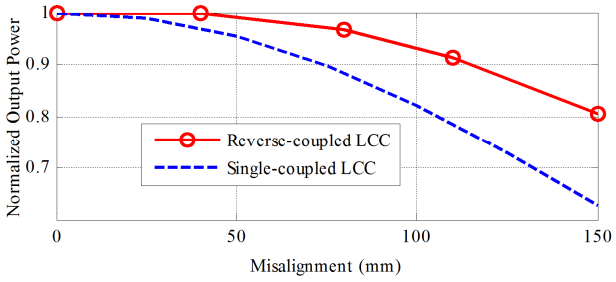

Fig. 13. Comparison of normalized output power in a reverse-coupled LCC system and a single-coupled LCC system

are shown in Fig. 11. It indicates that the system can still maintain near unity power factor and soft-switching at 150mm misalignment case. When the misalignment increases from zero to 150mm, the system power and efficiency are also measured and shown in Fig. 12. It shows that the system has very good performance. When the misalignment is within 80mm, the system power and efficiency are not affected at all. When the misalignment increases to 150mm, the system drops to 1.73kW with 89.1% efficiency. The angular misalignment performance is also tested. When the receiver rotates all the way from zero to 360°, the system power and efficiency are not affected.

The misaligned performance of this proposed reverse-coupled LCC-compensated system is also compared with the conventional single-coupled LCC-compensated system as shown in Fig. 13. The red curve represents the normalized output power of the reverse-coupled IPT system, which comes from experiments. The blue curve represents the normalized output power of the single-coupled IPT system, which is proportional to the coupling coefficient in Fig. 6. It shows that the designed system can maintain 80.5% of the well-aligned power at 150mm misalignment case, which is much better than the single-coupled system.

V. CONCLUSION

A reverse-coupled bipolar coil structure is proposed in this paper, which can improve both the position and angular misalignment performance of an IPT system. The system working principle and the reverse-coupled structure are discussed in detail. A prototype is implemented to validate the proposed system. Experiments shows that it achieves 2150W power transfer with 89.9% dc-dc efficiency across an airgap of 200mm, and 80.5% of the well-aligned power is maintained at 150mm misalignment.

REFERENCES

[1] J. Feng, Q. Li, F. Lee, "Omnidirectional Wireless Power Transfer for Portable Devices," *IEEE Applied Power Electronics Conference* (*APEC*), pp. 1675-1681, 2017.

[2] F. Lu, H. Zhang, H. Hofmann, C. Mi, "A Dynamic Charging System with Reduced Output Power Pulsation for Electric Vehicles," *IEEE Trans. Ind. Electron.*, vol. 63, no. 10, pp. 6580-6590, 2016.

[3] R. Bosshard, J. W. Kolar, "Multi-Objective Optimization of 50 kW/85 kHz IPT System for Public Transport," *IEEE J. Emerg. Sel. Top. Power Electron.*, vol. 4, no. 4, pp. 1370-1382, 2016.

[4] R. Bosshard, J. W. Kolar, "Inductive Power Transfer for Electric Vehicle Charging: Technical Challenges and Tradeoffs," *IEEE Power Electron. Mag.*, vol. 3, no. 3, pp. 22-30, 2016.

[5] S. Li, C. Mi, "Wireless Power Transfer for Electric Vehicle Applications," *IEEE J. Emerg. Sel. Top. Power Electron.*, vol. 4, no. 4, pp. 4-17, 2015.

[6] Y. Sohn, B. Choi, E. Lee, G. Lim, G. Cho, C. Rim, "General Unified Analyses of Two-Capacitor Inductive Power Transfer Systems: Equivalence of Current-Source SS and SP Compensations," vol. 30, no. 11, pp. 6030-6045, 2015.

[7] J. Acero, J. Serrano, C. Carretero, I. Lope, J. Burdio, "Analysis and Design of Tubular Coils for Wireless Inductive Power Transfer Systems," *IEEE Applied Power Electronics Conference* (*APEC*), pp. 848-854, 2017.

[8] M. Lu, K. Ngo, "Comparison of Passive Shields for Coils in Inductive Power Transfer," *IEEE Applied Power Electronics Conference* (*APEC*), pp. 1419-1424, 2017.

[9] J. Deng, F. Lu, S. Li, T.D. Nguyen, C. Mi, "Development of a High Efficiency Primary Side Controlled 7kW Wireless Power Charger," in *Proc. IEEE Intern. Elec. Veh. Conf. (IEVC)*, pp. 1-6, 2014.

[10] S. Wang, J. Chen, Z. Hu, C. Rong, M. Liu, "Optimisation design for series–series dynamic WPT system maintaining stable transfer power," *IET Trans. Ind. Electron.*, vol. 10, no. 9, pp. 987-995, 2017.

[11] Y. Wang, Y. Yao, X. Liu, D. Xu, "S/CLC Compensation Topology Analysis and Circular Coil Design for Wireless Power Transfer," *IEEE Trans. Trans. Electrif.*, vol. 3, no. 2, pp. 496-507, 2017.

[12] S. Li, W. Li, J. Deng, T.D. Nguyen, C. Mi, "A Double-sided LCC Compensation Network and Its Tuning Method for Wireless Power Transfer," *IEEE Trans. Veh. Technol.*, vol. 64, no. 6, pp. 2261-2273, 2015.

[13] R. Bosshard, U. Iruretagoyena, J. W. Kolar, "Comprehensive Evaluation of Rectangular and Double-D Coil Geometry for 50 kW/85 kHz IPT System," *IEEE J. Emerg. Sel. Top. Power Electron.*, vol. 4, no. 4, pp. 1406-1415, 2016.

[14] M. Budhia, J.T. Boys, G.A. Covic, C.Y. Huang, "Development of a Single-sided Flux Magnetic Coupler for Electric Vehicle IPT Charging Systems," *IEEE Trans. Ind. Electron.*, vol. 60, no. 1, pp. 318-328, 2013.

[15] S.Y. Choi, S.Y. Jeong, E.S. Lee, B.W. Gu, S.W. Lee, C.T. Rim, "Generalized Models on Self-Decoupled Dual Pick-up Coils for Large Lateral Tolerance," *IEEE Trans. Power Electron.*, vol. 30, no. 11, pp. 6434-6445, 2015.

[16] J. Deng, F. Lu, W. Li, R. Ma, C. Mi, "ZVS Double-Side LCC Compensated Resonant Inverter with Magnetic Integration for Electric Vehicle Wireless Charger," *IEEE Applied Power Electronics Conference* (*APEC*), pp. 1131-1136, 2015.

[17] W. Li, H. Zhao, J. Deng, T. Kan, C. Mi, "Integrated LCC Compensation Topology for Wireless Charger in Electric and Plug-in Electric Vehicles," *IEEE Trans. Ind. Electron.*, vol. 62, no. 7, pp. 4215-4225, 2015.

[18] T. Kan, T.D. Nguyen, J.C. White, R.K. Malhan, C. Mi, "A New Integration Method for an Electric Vehicle Wireless Charging System Using LCC Compensation Topology: Analysis and Design," *IEEE Trans. Power Electron.*, vol. 32, no. 2, pp. 1638-1650, 2017.

[19] F. Lu, H. Zhang, T. Kan, H. Hofmann, Y. Mei, L. Cai, C. Mi, "A High Efficiency and Compact Inductive Power Transfer System Compatible with Both 3.3kW and 7.7kW Receivers," *IEEE Applied Power Electronics Conference* (*APEC*), pp. 3669-3673, 2017.

[20] F. Lu, H. Zhang, H. Hofmann, C. Mi, "A Dual-Coupled LCC-Compensated IPT System to Improve Misalignment Performance," in *Proc. IEEE Workshop on Emerging Technologies: Wireless Power Transfer* (*WoW*), pp. 1-8, 2017.

[21] F. Lu, H. Zhang, H. Hofmann, W. Su, C. Mi, "A Dual-Coupled LCC-Compensated IPT System with a Compact Magnetic Coupler," *IEEE Trans. Power Electron.*, 2017, doi: 10.1109/TPEL.2017.2748391.